Optical Materials 149 (2024) 115014

Contents lists available at ScienceDirect

Optical Materials

journal homepage: www.elsevier.com/locate/optmat

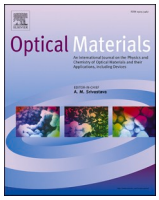

Research Article

Organic soluble nitrogen-doped carbon dots (ONCDs) to reduce the optical band gap of PVC polymer: Breakthrough in polymer composites with improved optical properties

Sewara J. Mohammed [a,b,*], Farouq E. Hawaiz [c], Shujahadeen B. Aziz [d,e], Sabah H Al-Jaf [f]

[a] Anesthesia Department, College of Health Sciences, Cihan University Sulaimaniya, Sulaimaniya, 46001, Kurdistan Region, Iraq
[b] Department of Chemistry, College of Science, University of Sulaimani, Qlyasan Street, Sulaimani, 46002, Kurdistan Regional Government, Iraq
[c] Department of Chemistry, College of Education, Salahaddin University – Hawler, Erbil, Kurdistan, Iraq
[d] Research and Development Center, University of Sulaimani, Qlyasan Street, Kurdistan Regional Government, Sulaymaniyah, 46001, Iraq
[e] Department of Physics, College of Science, Charmo University, 46023, Chamchamal, Sulaymaniyah, Iraq
[f] Department of Chemistry, College of Science, University of Garmian, Darbandikhan Road, 46021, Kalar City, Sulaimaniyah Province Kurdistan, Iraq

ARTICLE INFO

Keywords:
Nitrogen-doped carbon dots
Solvent-free synthesis
Mechanism formation
Spectroscopic analysis
PVC/ONCDs composite films
Optical band gap reduction

ABSTRACT

Polyvinyl chloride (PVC) is a common thermoplastic polymer with limited optical applications due to its large optical band gap. In this study, organic soluble nitrogen-doped carbon dots (ONCDs) were synthesized from 4-aminoantipyrine (4AA) as the precursor through a solvent-free method and employed to reduce the optical band gap of PVC polymer considerably. The formation of ONCDs was investigated through spectroscopic analysis. The synthesized ONCDs were characterized using various techniques, including FTIR, XPS, ^{13}C NMR, ^{1}H NMR, UV–Vis spectroscopy, PL spectroscopy, HR-TEM, and XRD. FTIR and XPS analyses identified the existence of amine, imine, and hydroxy groups on the surface of ONCDs. Furthermore, XPS analysis revealed the presence of carbon, nitrogen, and oxygen via distinguished peaks. ^{13}C NMR and ^{1}H NMR spectra supported the formation of ONCDs. UV–Vis, PLE, and PL spectroscopy techniques provided insights into the light absorption and emission properties of ONCDs. HR-TEM analysis showed uniform ONCDs with a mean particle size of 9 nm. XRD analysis confirmed an amorphous nanostructure of ONCDs with 0.42 nm interlayer spacing. The results illustrate that the absorption of photons by the PVC/ONCDs films covers the entire range of UV to near-infrared. The refractive index was tuned from 1.72 to 2.16 upon adding ONCDs. The increase of the optical dielectric constant (ε_1) is attributed to the increase in the localized density of states (N/m*). Based on quantum concepts, the optical dielectric loss (ε_2) was examined to determine the exact value of energy gaps. Taucs model along ε_2 results was utilized to determine the type of electron transition. The PVC/ONCDs films display a low band gap within the range of 1.52–1.78 eV. These findings demonstrate that the PVC/ONCDs films have improved optical properties and potential for various optoelectronic applications.

1. Introduction

A recent study revealed that materials exhibit different electrical and optical properties at the nanoscale than at the macroscale [1]. Polymer composites and synthetic polymers have become increasingly popular in various industries and applications due to their unique properties and versatility [2,3]. Among them, Polyvinyl chloride (PVC), a synthetic thermoplastic polymer, has remarkable physical attributes, such as high mechanical strength, chemical resistance, low flammability, low cost, and high availability [4,5]. These make PVC one of the most common polymers for various industrial and commercial applications, including packaging, construction materials, and medical devices [6]. However, PVC's large optical band gap restricts its application in some optoelectronic and photovoltaic devices, such as solar cells and light-emitting diodes. To address this challenge, researchers have tried different methods, such as adding organic and inorganic compounds as composite materials, to reduce the optical band gap of PVC [7].

In polymer science and technology, the use of reinforced PVC composites has grown recently [8,9]. Organic-inorganic composites have been developed for novel optical and electrical devices, nonlinear optics,

* Corresponding author. Anesthesia Department, College of Health Sciences, Cihan University Sulaimaniya, Sulaimaniya, 46001, Kurdistan Region, Iraq.
E-mail address: Sewara.mohammed@univsul.edu.iq (S.J. Mohammed).

https://doi.org/10.1016/j.optmat.2024.115014
Received 26 July 2023; Received in revised form 13 January 2024; Accepted 30 January 2024
Available online 5 February 2024

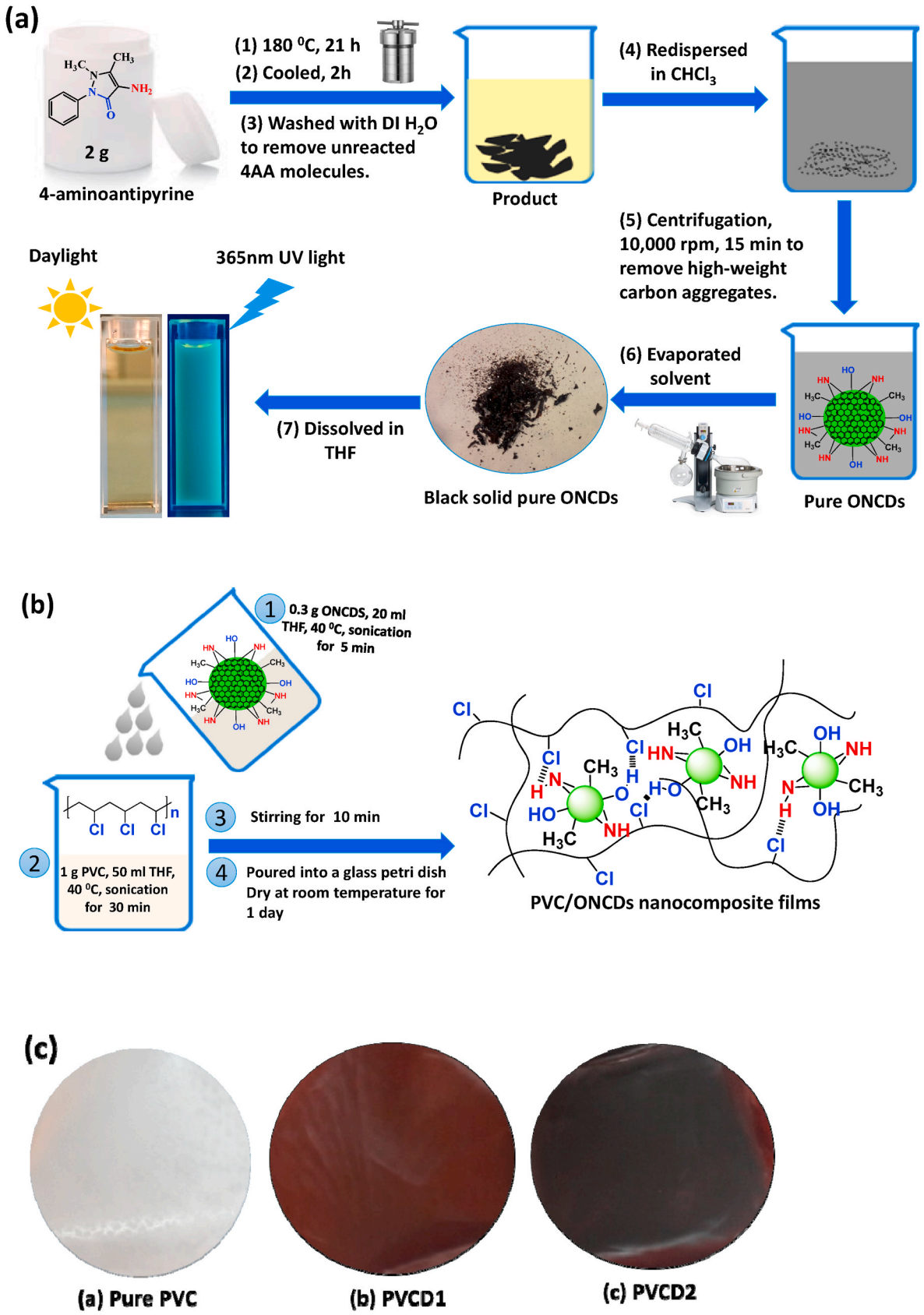

Scheme 1. Synthesis of the ONCDs and PVC/ONCDs films. (a) The schematic diagram of the solvent-free technique for synthesizing ONCDs from 4-aminoantipyrine (b) synthesis of nanocomposite (PVC/ONCDs) films and some possible interactions between the PVC chains and ONCDs. (c) Photographs of (a) pure PVC, (b) PVC/ONCDs 0.3 g, and (c) PVC/ONCDs 0.6 g.

and biological labeling purposes [10]. Another strategy to reduce the optical band gap of polymers is to add carbon dots to the polymer matrix, taking advantage of the unique optical and electrical properties of these nanomaterials [11,12]. Carbon dots (CDs) represent a novel type of carbon nanomaterials, typically characterized by their size, which is usually below 10 nm [13]. CDs contain abundant nitrogen, oxygen, and hydrogen-containing species on their surfaces, such as –OH, NH_2, and –COOH, which are utilized as fillers to enhance hydrogen bonds [14]. CDs can be synthesized by top-down or bottom-up methods using various carbon sources, such as carbon black, graphite, carbon nanotubes, small organic molecules, and natural products. Chemical or physical techniques, such as hydrothermal, microwave-assisted, or chemical methods, are also used for synthesis [15]. One of the most essential methods of synthesizing carbon dots is a solvent-free approach that avoids using solvents and reduces the environmental impact of the synthesis process. The solvent-free approach offers several advantages, including simplicity, cost-effectiveness, and scalability, making it a promising method for the large-scale production of carbon dots [16,17].

Carbon dots' unique optical and electronic properties make them potential candidates for a wide range of applications in optoelectronics [18,19]. CDs offer biocompatibility, high photostability, low toxicity, and exceptional water solubility, rendering them well-suited for various biological applications, including bioimaging and drug delivery [20,21]. Moreover, their tunable photoluminescence and excellent photoelectric properties make them promising for sensors, light-emitting diodes, and solar cells [22,23]. Additionally, C-dots are chemically stable, inert, produce a stable colloidal solution, and are remarkably resistant to photobleaching compared to ordinary fluorescent organic dyes and semiconductor quantum dots [24]. Incorporating CDs into polymer matrices can enable numerous photonic and optoelectronic applications and practical device integration, which is an active area of research [25].

Based on the information, the present study used a solvent-free method to synthesize ONCDs from 4-aminoantipyrine. These ONCDs were incorporated into polyvinyl chloride (PVC) via a solution cast technique to create composite films. The resulting PVC/ONCDs composite films demonstrated improved optical properties, particularly a decrease in the optical band gap of the PVC polymer. This suggests that these composite films could have potential applications in optoelectronics.

2. Experimental section

2.1. Materials

4-aminoantipyrine and polyvinyl chloride were obtained from Sigma-Aldrich. Deionized water was utilized to purify the ONCDs. Organic solvents, specifically chloroform ($CHCl_3$) and tetrahydrofuran (THF), were sourced from Tianjin Fengchuan Chemical Reagent Technology Co., Ltd. (Tianjin, China). Commercially available reagents and solvents were obtained and directly used in the study without any further purification steps.

2.2. Instrumental analysis

Utilizing a Perkin-Elmer spectrophotometer (Waltham, Massachusetts, USA), the FT-IR spectra were acquired with KBr pellets. The Bruker DRX-500MHz instrument (Billerica, Massachusetts, USA) was used to measure the ^1H NMR and ^{13}C NMR spectra in DMSO-d_6 and $CDCl_3$ solvents. The chemical shifts were expressed in parts per million (ppm) relative to the residual solvent peak, with reference values of 7.26 ppm for $CDCl_3$ and 2.5 ppm for DMSO-d_6. The Thermo Scientific K-Alpha X-Ray Photoelectron Spectrometer was employed to acquire X-ray photoelectron spectroscopy (XPS) spectra. Absorption spectra in the UV–vis range were gathered using an Agilent Technologies Cary 60 Spectrophotometer. At the same time, measurements of photoluminescence (PL) emissions were conducted on an Agilent Technologies Cary Eclipse fluorescence spectrophotometer. PLQY (Φ) was determined by calculating the photoluminescence quantum yield of ONCDs compared to the reference fluorescein (Φ = 0.92). X-ray diffraction (XRD) patterns were recorded using a Panalytical Empyrean X-ray diffractometer. The morphology and microstructure analysis was performed using high-resolution transmission electron microscopy (HRTEM) with an accelerating voltage of 200 kV on an FEI TEC9G2 microscope.

2.3. Synthesis of ONCDs

High-quality ONCDs were effectively synthesized using a solvent-free technique, employing 4-aminoantipyrine (4AA) as the only precursor. The synthesis involved self-dehydration condensation of functional groups in the starting material, conducted under elevated temperature conditions as depicted in Scheme 1a. The experiment was started by adding 2 g of 4AA to a 25 mL stainless-steel autoclave coated with Teflon. Subsequently, the autoclave was subjected to a constant temperature of 180 °C for 21 h. The reaction mixture was left to cool down naturally to room temperature, forming a highly viscous, dark black liquid. The product was rinsed with deionized water thrice to eliminate any leftover unreacted 4AA molecules. Subsequently, the obtained product was re-dispersed in chloroform and subjected to centrifugation at 10,000 rpm for 15 min to eliminate large carbon aggregates. Finally, 1 g of black solid ONCDs was obtained by evaporating the solvent using a rotary evaporator under reduced pressure. The ONCDs were characterized and preserved at room temperature for future utilization.

2.4. Synthesis of (PVC/ONCDs) nanocomposite films

Under ultrasonic irradiation, nanocomposite films were synthesized using the solution casting method. The procedure is described below and illustrated in Scheme 1b. First, a solution of PVC was prepared by dissolving 1 g of PVC in 50 ml of tetrahydrofuran (THF) under ultrasonic radiation at 40 °C for 30 min until a clear solution was obtained. Next, two different concentrations (0.3 g and 0.6 g) of ONCDs were dissolved in 20 mL of THF using ultrasonic radiation for 5 minutes at 40 °C, ensuring a uniform ONCDs solution. The ONCDs solutions were then added to a container containing the PVC solution. The mixture was vigorously stirred at room temperature for 10 minutes using a magnetic stirrer to attain a homogeneous solution. Subsequently, the solution was transferred into a glass petri dish and kept at room temperature for 24 hours. This allowed the formation of a dry film with excellent homogeneity. The resulting films were labeled as Pure PVC, PVCD1, and PVCD2, indicating the incorporation of PVC solutions containing 0 g, 0.3 g, and 0.6 g of ONCDs, respectively. Photographs of the PVCD films with varying ONCD contents are displayed in Scheme 1c.

3. Results and discussion

3.1. Synthesis, mechanism formation, and characterization of ONCDs

The synthesis of ONCDs was accomplished using a solvent-free method, employing 4-aminoantipyrine as the precursor, resulting in an impressive yield of 50 % and a quantum yield of 10 %. The synthesis process relied on self-condensation reactions and noncovalent π-π stacking interactions, which were carried out at 180 °C for 21 hours. Notably, this method eliminated the need for solvents or additional precursors, enhancing the efficiency of the process. Reasons for choosing 4AA as the precursor include its readily available nature, high carbon content, and presence of carbonyl and amine groups. The mechanism of ONCDs formation can be elucidated through spectroscopic analysis. Self-condensation reactions were aided by the carbonyl and amine groups in 4-aminoantipyrine and the lack of water throughout the

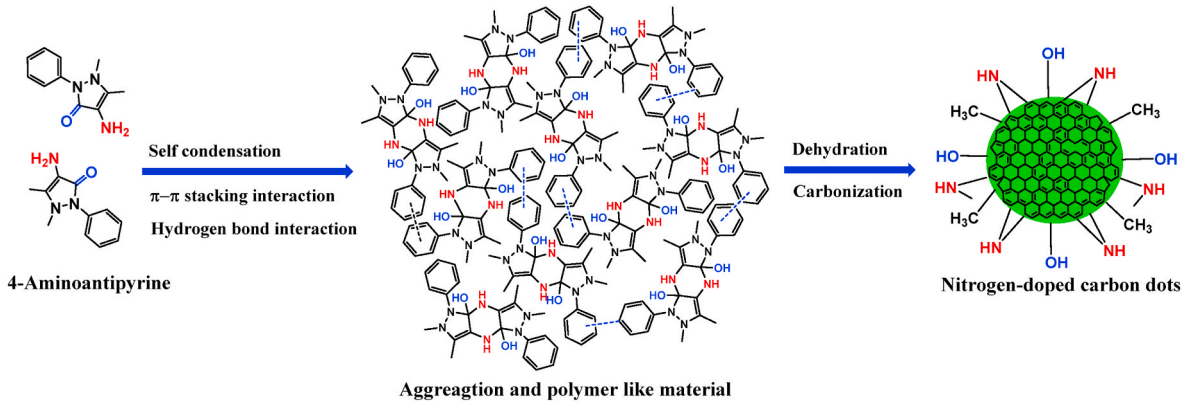

Fig. 1. Proposed mechanism for the synthesis of ONCDs.

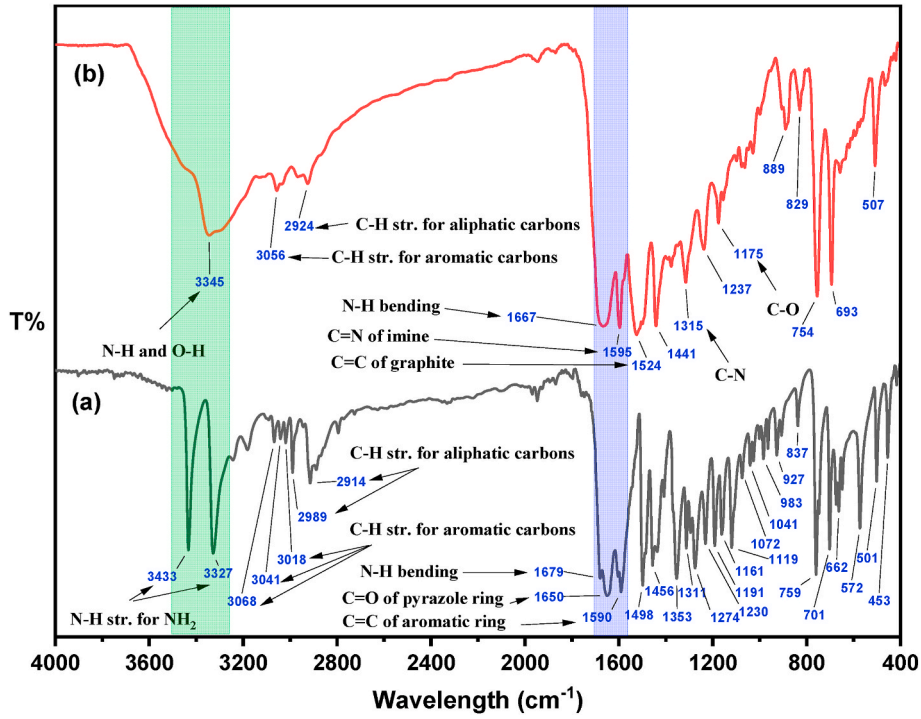

Fig. 2. FTIR spectra of both 4AA and ONCDs.

process [26]. Furthermore, the benzene ring, hydroxy, and amine groups in 4-aminoantipyrine enabled inter and intra-molecular hydrogen bonding and noncovalent π-π stacking interactions, forming polymer-like material [27,28]. Subsequently, elevated temperatures induced significant water removal, initiating the carbonization process and forming a carbon core. The remaining amino and hydroxy groups in 4-aminoantipyrine became localized on the carbon surface after the carbon core formation. This localization resulted in the generation of surface charges on the surface of the nitrogenous carbon dots, as illustrated in Fig. 1. Various techniques were employed to analyze the synthesized ONCDs, such as FTIR, XPS, ^{13}C NMR, ^{1}H NMR, UV–Vis spectroscopy, PL spectroscopy, HR-TEM, and XRD.

3.1.1. FT-IR characterization of the ONCDs

The surface functional groups of the synthesized ONCDs were investigated through FTIR analysis. Fig. 2 depicts the FTIR spectrum of both 4AA and ONCDs. Notably, the ONCDs exhibited distinct peaks at 3345, 1667, 1595, and 1524 cm^{-1}, indicating the presence of specific functional groups. These peaks corresponded to the N–H stretching of amine or/and O–H stretching of alcohol, the –NH bending of amine, the –C═N of imine, and the –C═C- of aromatic rings, respectively. Additionally, the ONCDs displayed peaks at 3056 and 2924 cm^{-1}, signifying the C–H stretching of aliphatic and aromatic rings, respectively. Furthermore, the presence of C–N and C–O groups on the ONCDs surface was suggested by two additional peaks at 1315 and 1175 cm^{-1}. Interestingly, the absence of NH_2 and C═O peaks at wavenumbers of 3432 and 3327 cm^{-1} and 1655 cm^{-1}, respectively, in the pyrazole ring of 4AA, suggested that self-condensation reactions occurred during the carbonization process. As a result, the fundamental structure of 4AA was not preserved in the ONCDs' structure [29]. The FTIR analysis revealed the existence of amine, hydroxyl, and amine groups on the ONCDs' surface. These results were corroborated by X-ray photoelectron spectroscopy (XPS).

3.1.2. XPS characterization of the ONCDs

X-ray photoelectron spectroscopy (XPS) was used as a characterization tool to provide insights into the elemental composition and chemical bonding states of the ONCDs. In Fig. 3a, the XPS survey spectrum is

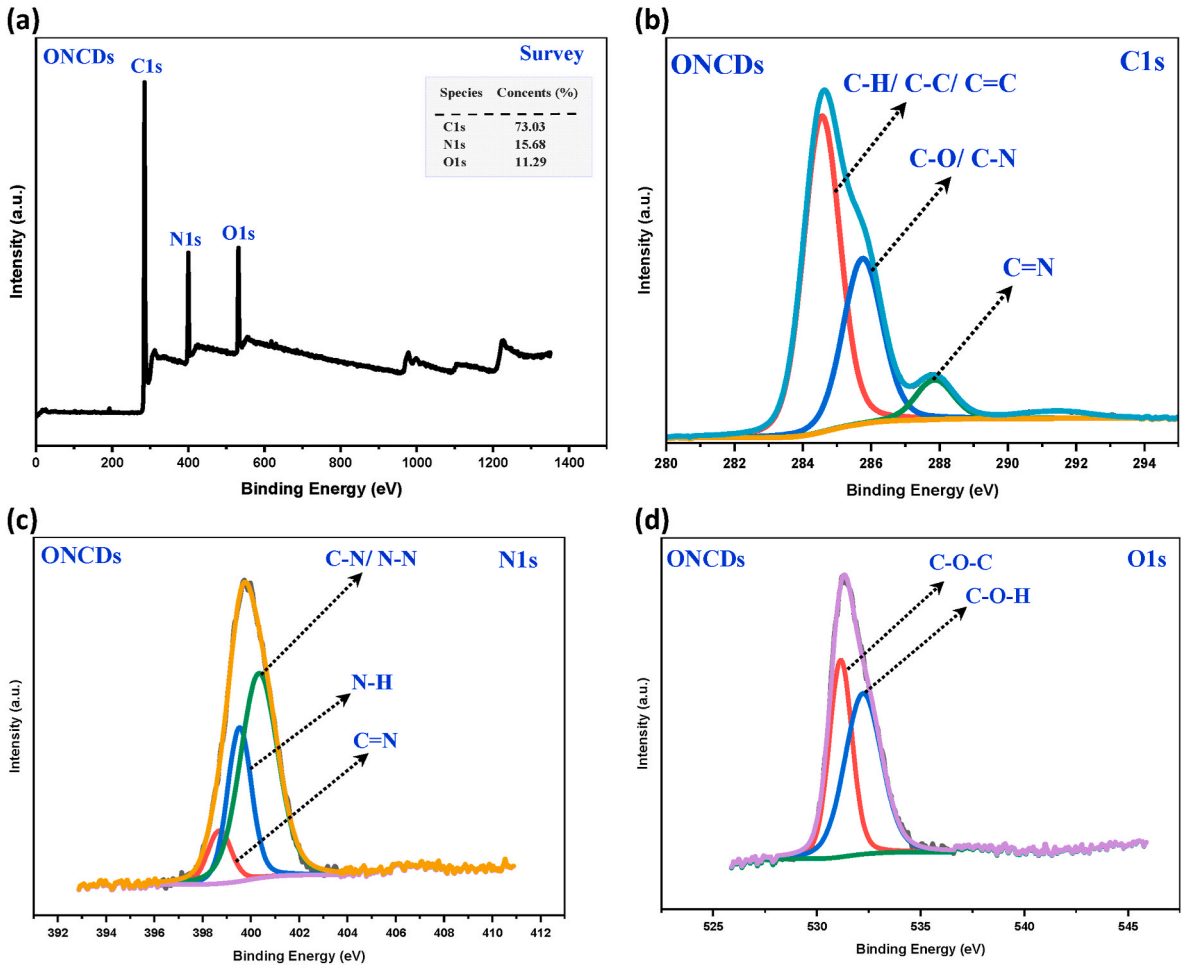

Fig. 3. XPS results for ONCDs, with (a) showing the overall survey spectrum, and the detailed high-resolution spectra of C 1s, N 1s, and O 1s are represented in (b), (c), and (d) respectively.

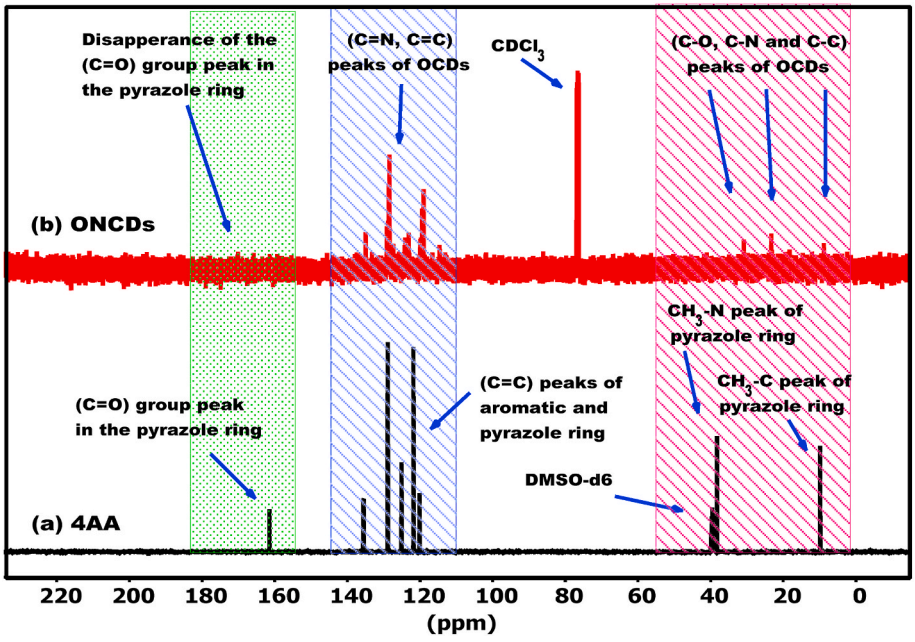

Fig. 4. ^{13}C NMR spectra of 4AA and ONCDs.

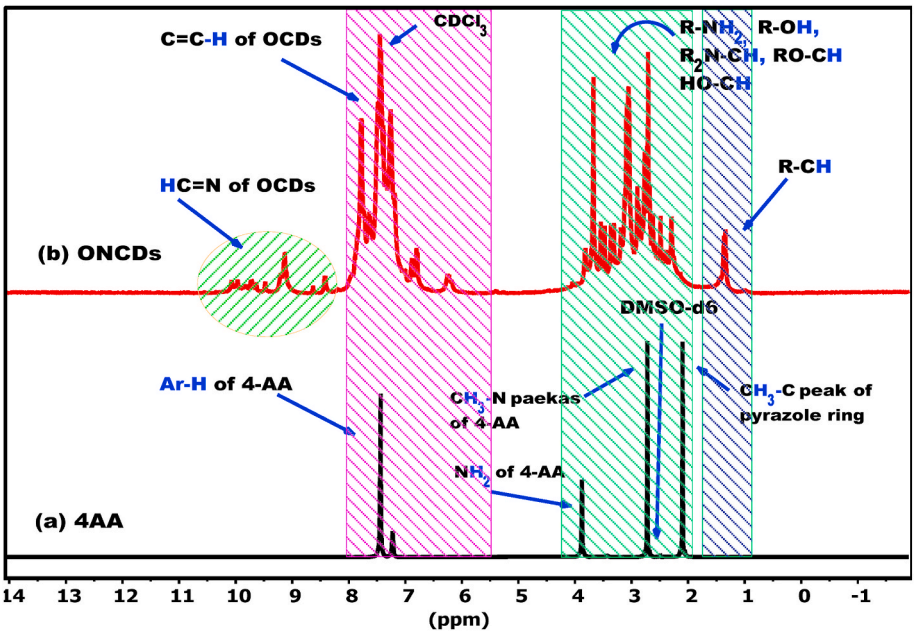

Fig. 5. ^{1}H NMR spectra of 4AA and ONCDs.

displayed, confirming the existence of carbon, nitrogen, and oxygen elements in the ONCDs. This was supported by identifying peaks at specific energy levels, namely C 1s at 284.7 eV, N 1s at 399.8 eV, and O 1s at 531.3 eV [30]. Detailed examination of the ONCDs was conducted through high-resolution spectra. Fig. 3b exhibited the high-resolution C 1s spectrum of the ONCDs, which exhibited clear and separate peaks at specific energy levels. The peak at 284.5 eV indicated the presence of (C–H/C–C/C═C) bonding configurations. The peak at 285.7 eV also denoted (C–O/C–N) bonding configurations, while the peak at 287.8 eV signified (C═N) bonding configurations within the ONCDs. Likewise, in Fig. 3c, the high-resolution N 1s spectrum exhibited three distinct peaks at different energy levels, indicating the presence of specific chemical bonds in the ONCDs. The peak at 398.7 eV signified the occurrence of (C═N) bonds, while the peak at 399.5 eV was attributed to (N–H) bonds. Additionally, the peak at 400.3 eV confirmed the presence of (C–N/N–N) bonds in the ONCDs [31,32]. In Fig. 3d, the O 1s spectrum of the ONCDs demonstrated two distinct peaks. The first peak, at 531.1 eV, indicated the presence of C–*O*–C bonding, while the second peak, at 532.2 eV, corresponded to C–O–H bonding. The ^{13}C NMR and ^{1}H NMR spectra analysis further supported the formation of ONCDs through self-condensation reactions.

3.1.3. ^{13}C NMR characterization of the ONCDs

The ^{13}C NMR spectra of both 4AA and ONCDs are presented in Fig. 4 and Figs. S1a and S1b of the supporting information. In the ^{13}C NMR spectrum of 4AA, a peak is observed at 161 ppm, corresponding to the carbonyl (C═O) group in the pyrazole ring. However, this peak disappeared in the spectra of ONCDs, indicating that self-condensation reactions occurred during the carbonization process, leading to the formation of ONCDs [29]. The ^{13}C NMR spectrum of the ONCDs showed resonance peaks at (119–135) ppm, which can be ascribed to the sp2-hybridized carbons (C═C) in the aromatic ring, as well as imine carbons (C═N) formed during the synthesis process [33].

Furthermore, new peaks were detected in the 9–31 ppm range, indicating aliphatic carbons linked to amine and hydroxyl groups within the ONCDs [34]. The formation of these functional groups occurs due to the carbonization process. On the contrary, 4AA shows two peaks at 34 and 9 ppm, suggesting that its original structure was not preserved.

3.1.4. ^{1}H NMR characterization of the ONCDs

Fig. 5 and Figs. S2a and S2b in the supporting information illustrate the ^{1}H NMR spectra of 4AA and ONCDs. The ^{1}H NMR analysis of ONCDs reveals the appearance of new peaks within the 8.4–10 ppm range, which can be attributed to the presence of HC═N imine protons. This confirms that self-condensation reactions of 4AA occurred during the

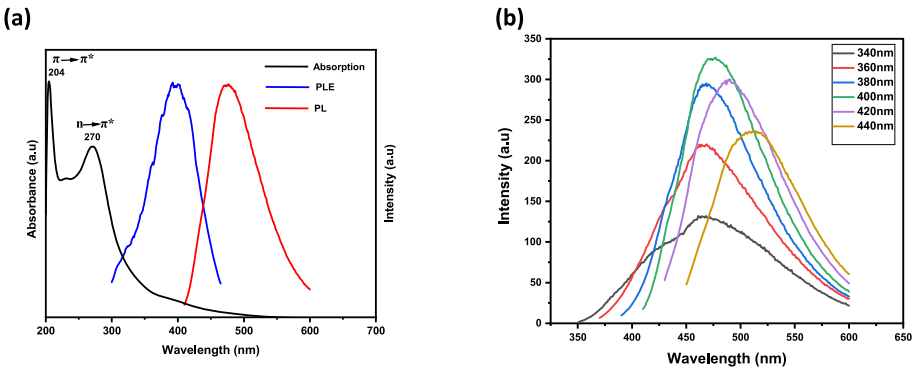

Fig. 6. (a) The UV–vis, PLE, and PL emission spectrum of the ONCDs dissolved in ethanol. (b) PL emission spectra of ONCDs under different excitation wavelengths, spanning from 340 to 440 nm.

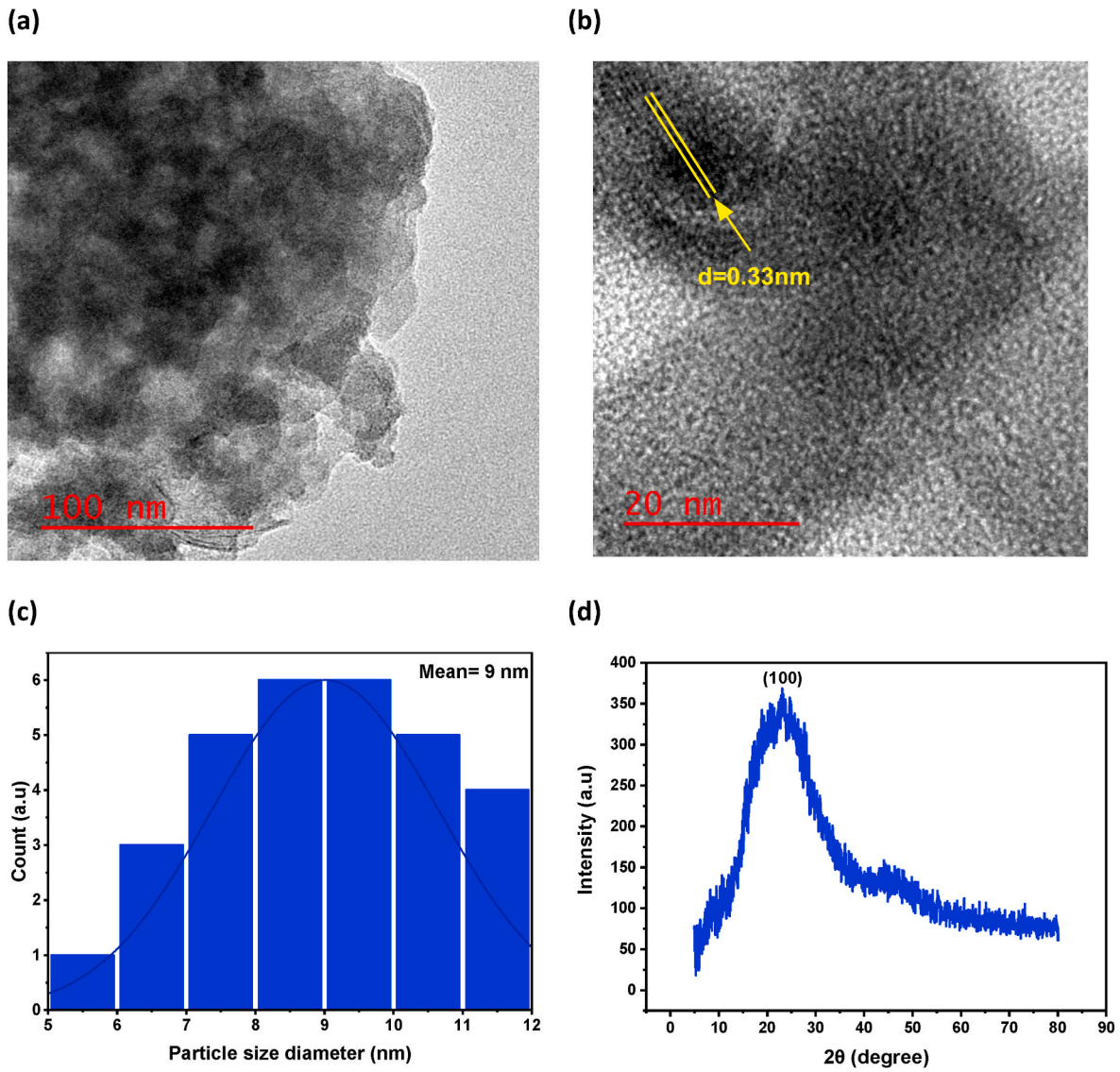

Fig. 7. HRTEM results of ONCDs at two dissimilar intensifications: (a) 100 nm and (b) 20 nm, revealing the presence of lattice fringes. (c) The particle size distribution histogram was derived from the image in (a) using a calculation method and n = 30, (d) XRD prototype of the ONCDs.

carbonization process, leading to the creation of ONCDs. Furthermore, the presence of a multiple of peaks between 6.7-7.8 ppm indicates the existence of aromatic and sp^2 protons. Additional new peaks ranging from 2.5 to 3.7 ppm were observed, corresponding to the C–H protons attached to the OH and NH groups formed during the carbonization process [35]. New peaks were identified within the 1.3 ppm range, representing the sp^3 C–H protons. Conversely, the N–CH_3 and C–CH_3 peaks from the 2.7 and 2.1 ppm ranges in the 4AA spectrum were no longer present [29]. This observation indicates that the fundamental structure of 4AA was not preserved during the transformation into ONCDs.

3.1.5. Optical properties of ONCDs

UV–visible (UV–vis), photoluminescence (PL) emission, and photoluminescence excitation (PLE) spectroscopy techniques were utilized to gain valuable insights into the light absorption and emission properties of ONCDs. The absorption, PL, and PLE spectra of ONCDs are illustrated in Fig. 6a and b. Two peaks were observed in the UV–visible spectrum of ONCDs (Fig. 6a). The first peak at a wavelength of 204 nm represented the $\pi \rightarrow \pi^*$ transition of the conjugated system of the ONCDs like (sp^2 aromatic/C═N and alkenyl C═C bonds). This indicates that the ONCDs have a strong conjugated structure with high electron density. The second absorption detected band at a wavelength of 270 nm corresponds to the $n \rightarrow \pi^*$ transition of the C═N bond [36,37]. Fig. 6a also presents the PLE spectrum, which exhibits a single PLE band at 400 nm. Furthermore, the PL emission spectrum exhibited a broad emission peak in the green region of the electromagnetic spectrum, with a central wavelength of approximately 480 nm [38], as illustrated in Fig. 6a. A substantial number of surface functional groups and the varied size distribution of the ONCDs impact this peak. To generate the photoluminescence (PL) emission spectrum of ONCDs, a range of excitation wavelengths from 340 to 440 nm was utilized, with increments of 20 nm, as demonstrated in Fig. 6b. The position of the PL emission peak of ONCDs varied depending on the excitation wavelength [39].

3.1.6. HR-TEM and XRD characterizations of ONCDs

High-resolution transmission electron microscopy (HR-TEM) was used to do a thorough analysis to improve our comprehension of the production process of ONCDs. This method allowed for an investigation into the structural properties and morphology of the ONCDs. The analysis of HR-TEM images determined the size distribution of the synthesized ONCDs, revealing an average particle size of 9 nm (Fig. 7c). The

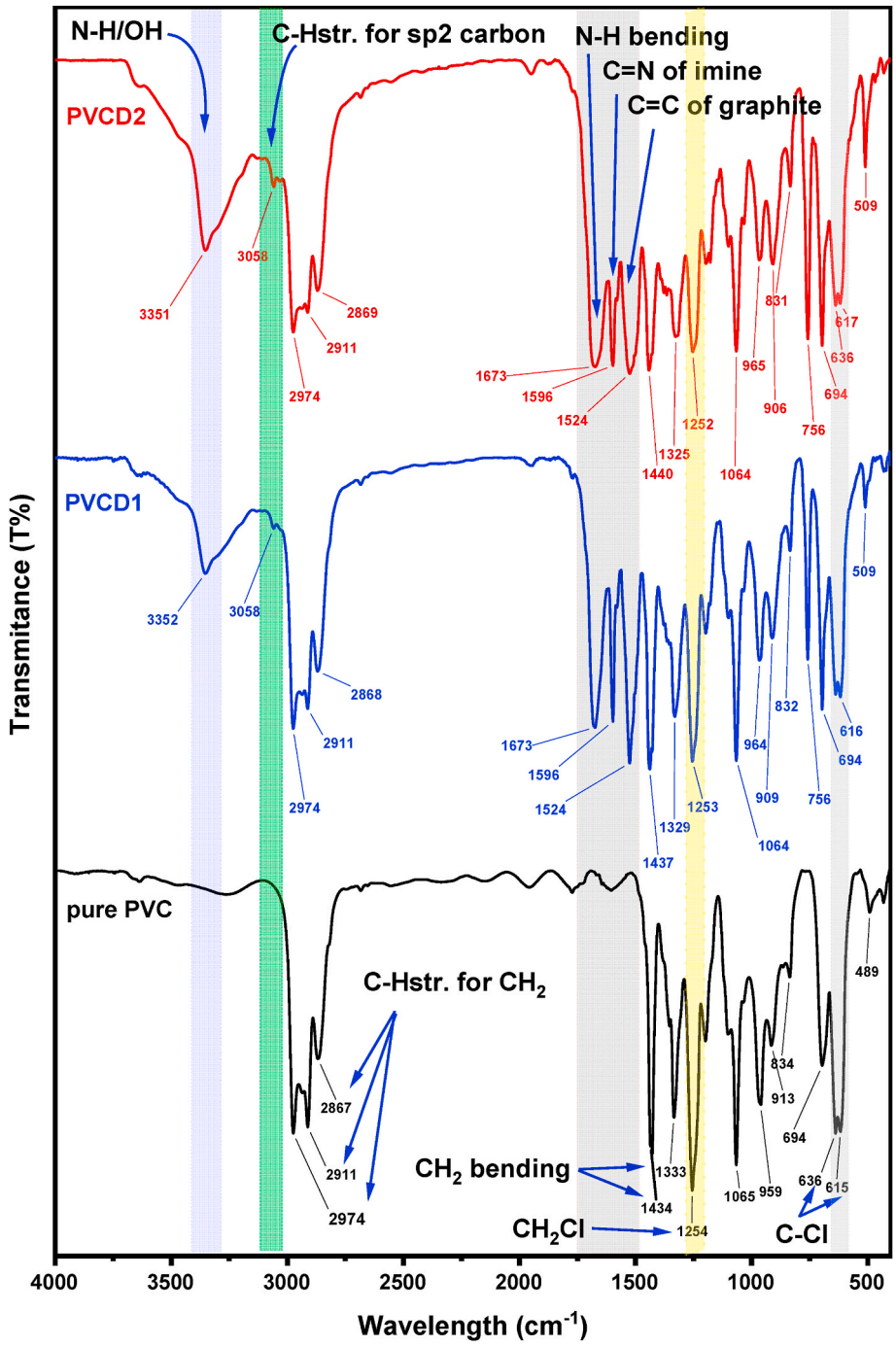

Fig. 8. FT-IR result of pure PVC and nanocomposites of PVC/ONCDs.

small and narrow size distribution indicated that the ONCDs exhibited uniformity in size and shape. Furthermore, the HR-TEM images provided valuable insights into the lattice structure of the ONCDs. Clear lattice fringes were observed, enabling the measurement of the interplanar spacing. The calculated d-space value was 0.33 nm, indicating the lattice spacing of the ONCDs (Fig. 7b) [40]. Significantly, this value corresponded to the (100) plane lattice of graphite carbon, suggesting the successful synthesis of ONCDs and implying their possession of unique optical and electronic properties. The well-defined lattice structure and uniform particle size distribution contribute to the potential influence of ONCDs on various applications. Additionally, X-ray diffraction (XRD) analysis was conducted to examine the crystal structure of the ONCDs. The XRD pattern displayed a prominent broad peak at 21.1° (Fig. 7d), indicating the presence of an amorphous structure [41]. Notably, the nitrogen-doped carbon dots displayed a d-spacing of 0.42 nm between their layers. These findings suggest that the ONCDs possess a layered nanostructure with a well-defined arrangement of carbon atoms and nitrogen dopants [42].

3.2. PVC/ONCDs nanocomposite films

3.2.1. FTIR study

The FT-IR spectra were utilized to enhance understanding of the chemical interactions and structural changes that occur when PVC and ONCDs are combined at various concentrations. Fig. 8 depicts the FT-IR spectra of both pure PVC and composites of PVC with ONCDs. The FT-IR

Table 1
Values of χc obtained through deconvoluted XRD analysis.

Sample	Degree of crystallinity (χc)
Pure PVC	20.68904
PVCD1	6.343771
PVCD2	2.209977

spectra of PVC exhibit distinct peaks around (2974-2867 cm^{-1} and 1434-1333 cm^{-1}), indicating the stretching and bending vibrations, respectively, of the CH_2 groups in the PVC backbone. The peak around 1254 cm^{-1} corresponds to the CH_2Cl groups exhibiting bending vibrations, while the peak in the range of 633-615 cm^{-1} arises from the stretching vibrations of the C–Cl bond in PVC [43]. In contrast, several new peaks appeared in the FT-IR spectra of PVC/ONCDs composites at 3352, 3058, 1673, 1596, and 1524 cm^{-1}, which are ascribed to OH/NH, C–H for sp2 carbon, N–H bending, imine form (C═N), and C═C, respectively. These findings suggest that PVC/ONCDs composites have been successfully prepared. In addition, the intensity peak at around 1434 cm^{-1} in pure PVC becomes shorter and shifts to a slightly higher wavenumber at around 1440 cm^{-1} in the PVC/ONCDs composite spectra, while the intensity peak at 1333 cm^{-1} becomes shorter and shifts to a slightly lower wavenumber at around 1325 cm^{-1}. This indicates some interactions between the CH_2 groups in PVC and ONCDs, which may cause some degree of crosslinking. Furthermore, the peaks of CH_2Cl and C–Cl in PVC at around (1254 and 636 cm^{-1}), respectively, become less intense in the PVC/ONCDs composite spectra, suggesting that the presence of ONCDs may influence the C–Cl bond in PVC. This phenomenon might be attributed to the hydrogen bond interaction between the hydrogen atoms of NH and OH groups in the ONCDs and the chlorine atoms in PVC. This interaction can alter the chemical composition and the composite's molecular structure.

3.2.2. XRD analysis

Through the existence of strong diffraction rings or peaks, X-ray diffraction (XRD) investigations give complete information regarding crystal structure, crystal orientation, crystallite size, and the existing material phases. Additionally, the amorphous materials have noticeable "halos" that are wide. The large peak from 2 = 17.38–26.02 reflects the amorphous characteristic of PVC in the virgin PVC film's XRD pattern [44,45]. In an earlier investigation, three halos were seen in the PVC film spectrum at 17.7°, 24.7°, and 40.6° [46]. We see that the position of the PVC reflection peaks remains the same; all of the distinctive XRD peaks are visible in the composite samples in the exact location as pure PVC regardless of the ONCDs concentration. However, the PCV major peaks have widened and lost some strength. On the other hand, the ONCDs particles distributed in PVC may significantly impact the PVC polymer's crystallization. This phenomenon might be attributed to the decreased chain-chain interactions caused by the interaction between ONCDs particles and the chlorine atom in the PVC polymer. Investigating the material's crystalline structure involved utilizing Origin 8 software to obtain the area under the crystalline and amorphous peaks. **Equation (1)** was employed to calculate the degree of crystallinity **(χc),** and the corresponding results are displayed in Table 1.

$$\chi_c = (A_C/A_T) \times 100\ \% \quad (1)$$

AT represents the total area of crystallized and amorphous peaks, while **AC** represents the area specifically attributed to crystallized peaks. Fig. 9 displays the Gaussian fitting results on PVC films. The **χc** values were determined by utilizing the **AT** and **AC** measurements, as indicated in Table 1. PVCD2 exhibits the highest amorphousness due to the increased amorphous phase resulting from the dispersions of ONCDs and interactions among PVC composite components [47].

3.2.3. Optical properties

3.2.3.1. Investigation of absorption characteristics. Fig. 10 displays the absorption spectra of both neat PVC and PVC/ONCDs films. There are two peaks visible in the ultraviolet range. Unlike unmodified PVC, the doped materials exhibit much more refined UV absorption. Molecular orbitals are employed to elucidate the absorption of light energy by polymers in the UV–visible spectrum, causing electrons in p, d, and n-orbitals to transition from the ground state to higher energy levels. Three different electronic transitions are possible: σ→σ*, n→π*, and π→π*. Doping materials with energies within the visible spectrum primarily initiate optical transitions, creating defects known as color centers [48]. Fig. 10 shows the spectra of neat PVC and PVC/ONCDs films, which have two peaks at about 211 nm and 281 nm (i.e., a broad shoulder peak) for pure PVC. The first one is ascribed to n-π*, while the second one could be attributed to π -π* transitions [49,50].

A useful method for researching electronic transitions is UV–vis. The comprehension of the energy band gap and band structure in both crystalline and non-crystalline materials is achieved through the examination of optical absorption spectra in solid substances [51]. Determining band strength or band-gap energy in non-crystalline materials can be accomplished by analyzing the absorption edge [52]. The absorption coefficient **(α)** of an optical media measures how much light it absorbs [53]. To obtain the absorption coefficient **(α),** equation **(2)** was employed.

$$\alpha_{(\lambda)} = (2.303/d)*A \quad (2)$$

where **A** is the data on absorption and **d** is the PVC film thickness. An incoming photon near the absorption edge causes an electron to transition from a lower to a higher energy state. The samples' amorphous nature is shown by an absorption coefficient that gradually increases with applied photon energy. Fig. 11 illustrates the variation of the absorption coefficient as a function of photon energy for pure PVC and PVC/ONCDs films. Table 2 displays the absorption edge values derived by extrapolating the linear portions of Fig. 11 to the X-axis. The absorption edge fluctuation in response to ONCDs insertion is redshifted from 4.75 eV to 1.6 eV. The absorption edge changes toward lower photon energy as ONCDs concentration rises. The shift in the absorption edge may be attributed to the forming of a conjugated bond system resulting from bond cleavage and subsequent reconstruction. This is a good turn of the structural and chemical alterations to PVC integrated with ONCDs [54]. The considerable alterations in absorption edge values prove that the band structure of PVC nanocomposites has changed.

3.2.3.2. Investigations of refractive index and optical dielectric constant. The optical refractive index **(n)**, which measures how much the speed of light is reducing in the material, is one of the parameters. Controlling the optical characteristics of materials depends on variations in the refractive indices of composite films. An earlier study found that examining the optical dielectric constant's real component (ε_1) and imaginary part (ε_2) is crucial for designing novel materials. The refractive index plays a vital role in the fabrication of prisms, optical windows, and optical fibers, serving as a critical optical property [55,56]. The refractive indices of the samples were determined using the reflectance **(R)** and extinction coefficient **(k)** values, employing **equation (3)** [57].

$$n = \left[\frac{(1+R)}{(1-R)}\right] + \sqrt{\frac{4\times R}{(1-R)^2} - K^2} \quad (3)$$

The extinction coefficient ($\mathbf{K = \alpha\lambda/4\pi t}$) is related to the absorption coefficient **(α),** the thickness of the PVC film **(d)**, and the wavelength **(λ).** The reflectance **(R)** was calculated using the absorption **(A)** and transmittance **(T)** values according to equation **R = 1 - (A + T).** The transmittance **(T)** values were derived from Beer's law as T = 10^(-A). The refractive index spectra of both pure PVC samples and doped

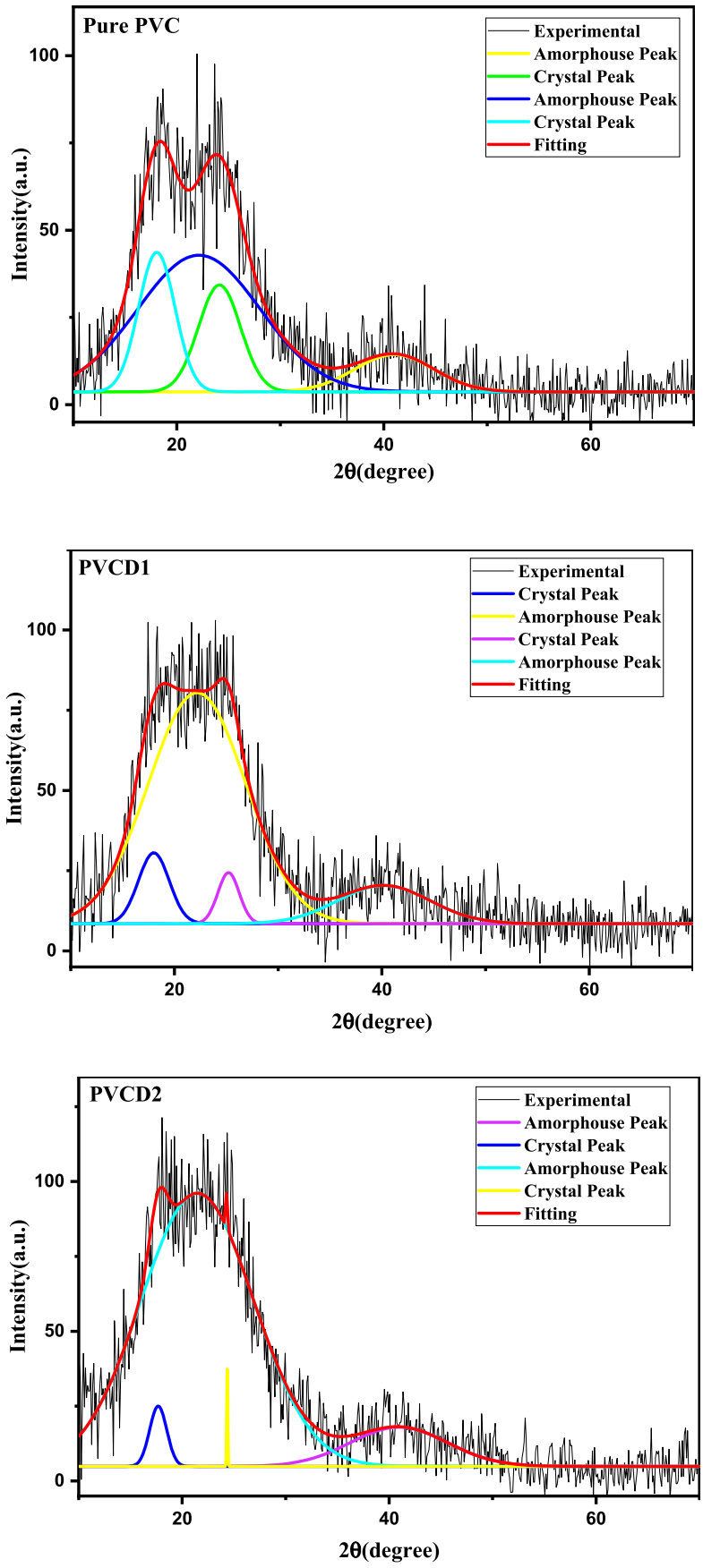

Fig. 9. XRD deconvolution for pure PVC and doped films.

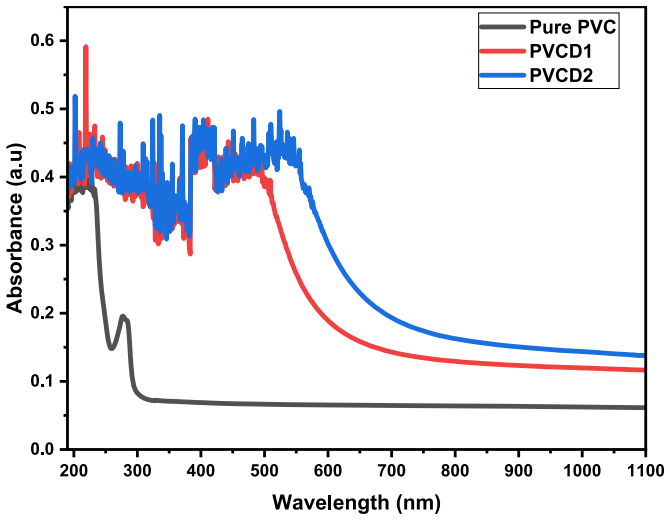

Fig. 10. Absorption spectra for pure and modified PVC films. The ONCDs improved the absorption behavior of PVC to cover the entire range of UV–visible.

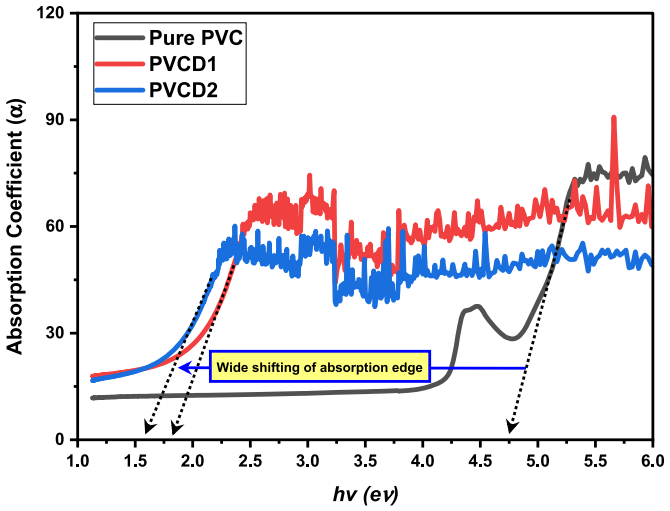

Fig. 11. Absorption coefficient spectra for pure and modified PVC films. The ONCDs decreased the absorption edge of PVC to the region close enough to semiconductor materials.

Table 2
Presents Absorption edge for PVC and PVC composites.

Sample	Absorption edge
Pure PVC	4.75
PVCD1	1.8
PVCD2	1.6

samples are depicted in Fig. 12. There is a clear correlation between the increase in ONCDs concentration and the corresponding rise in refractive index value (n), which escalated from 1.72 to 2.16. Following the renowned Lorentz-Lorenz formula, the host polymer matrix exhibits a greater refractive index once ONCDs are inserted, ascribing to the increase in charge carriers [58]. This is because the ONCDs make the matrix denser. Waveguides, light-emitting diodes, and antireflective coatings are a few examples of sophisticated optical and optoelectronic technologies that greatly benefit from high-refractive index materials

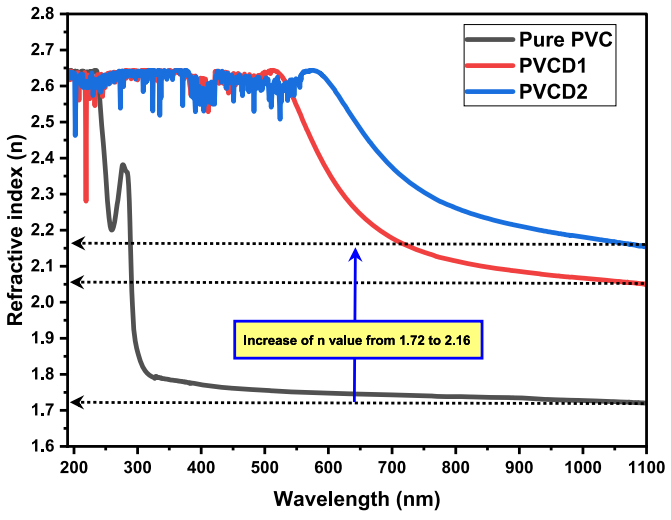

Fig. 12. Refractive index (n) spectra for pure and modified PVC films. The ONCDs improved the n value from 1.72 for pure PVC to 2.16 for PVC doped with ONCDs.

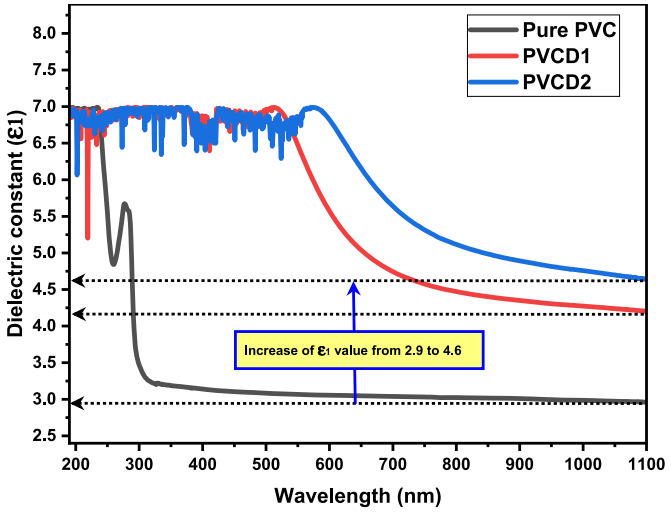

Fig. 13. The ε_1 spectra for pure and modified PVC films. The ONCDs improved the ε_1 value due to an increase in N/m*, thus increasing the number of electrons that can participate in the transition from VB to CB.

[59]. Additionally, compared to pure PVC, all doped films exhibit dispersion in the refractive index vs wavelength from the visible to near-infrared region.

Fig. 13 illustrates the plot of an important parameter, the optical dielectric constant **(ε_1)**. The ε_1 value is crucial to be studied because it is correlated with the localized density of states **(N/m*)**, as illustrated in **equation (4)**. Upon combining PVC with ONCDs material, a noticeable increase in the dielectric constant becomes apparent. This rise can be attributed to the increment in the density of states, as ε_1 is directly linked to the density of states within the band gap of the polymer films. Previous studies have revealed that the electronic component of the dielectric constant **(ε_1)** is strongly correlated with the optical band-gap [53]. This has a direct connection to the localized electronic states seen in materials' prohibited gaps [60]:

$$\varepsilon_1 = n^2 - k^2 = \varepsilon_\infty - \left(\frac{e^2}{4\pi^2\, C^2\, \varepsilon_o}\right) \times \left(\frac{N}{m^*}\right) \times \lambda^2 \quad (4)$$

Where $\boldsymbol{\varepsilon_\infty}$ represents the dielectric constant at longer wavelengths, while $\boldsymbol{\varepsilon_o}$ corresponds to the dielectric constant in free space. The symbol

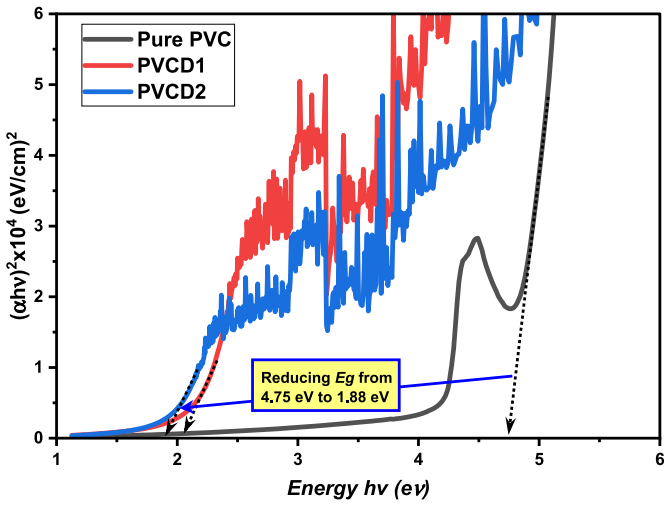

Fig. 14. The plot of $(\alpha h\upsilon)^{1/\gamma}$ versus photon energy is presented for a value of γ equal to 1/2.

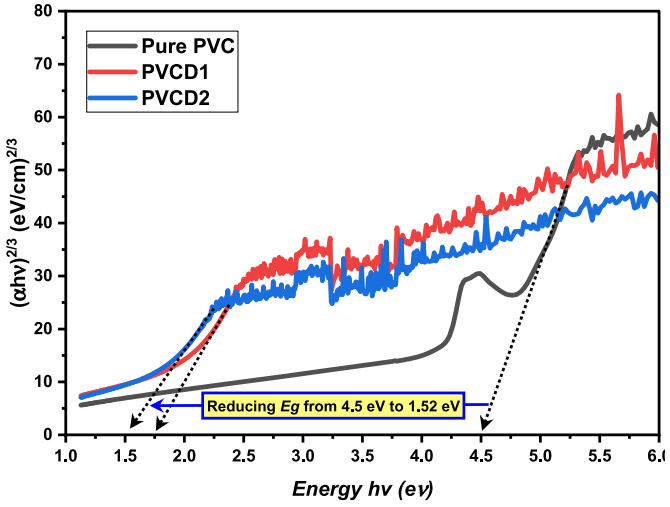

Fig. 15. The plot of $(\alpha h\upsilon)^{1/\gamma}$ versus photon energy is presented for a value of γ equal to 3/2.

e represents the electronic charge, while **C** denotes the speed of light. Fig. 13 depicts the wavelength dependence of the optical ε_1 value vs λ for different concentrations of ONCDs. Clearly, when the concentration of ONCDs is raised, the ε_1 values rise as well. The corresponding rise in the density of states **(N/m*)** is responsible for the increase in the ε_1 value, which goes from 2.9 to 4.6. When the optical dielectric constant is raised, more charge carriers are introduced, leading to a greater density of states.

3.2.3.3. Investigation of the optical band gap: Tauck's model and analysis of optical dielectric loss. UV–vis spectroscopy is commonly utilized as a standard method for determining the energy band gap of materials. The absorption of photon energy causes electron excitation, resulting in the development of an absorption edge. These deviations in the band gap energy provide insights into determining optical band gap energies [61]. Figs. 14 and 15 display the $(\alpha h\upsilon)^{1/\gamma}$ plots, while Fig. 16 illustrates the correlation between dielectric loss and photon energy **(hv)** for all the samples. The calculated band gap energy values for the samples can be obtained by analyzing the responses depicted in Figs. 14–16. The optical band gap can be determined using Tauc's **equation (5),** which relates the absorption coefficient as a function of photon energy [62,63].

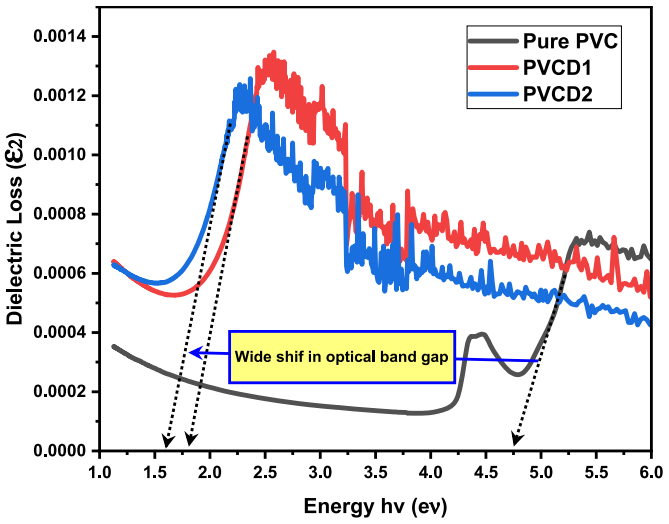

Fig. 16. The ε_2 spectra for pure and modified PVC films. The ONCDs reduced the energy gap from 4.76 eV to 1.51 eV value due to an increase in N/m*, thus increasing the number of electrons that transfer from VB to CB.

Table 3
Displays the band gap values obtained from the ε2 plot and Tauc's method.

Samples	= 1/2γ	= 3/2γ	From ε_2
Pure PVC	4.75	4.5	4.76
PVCD1	2.14	1.76	1.78
PVCD2	1.88	1.52	1.52

$$\alpha h\nu = B\left(h\nu - E_g\right)^{\gamma} \quad (5)$$

Where ***α*** represents the absorption coefficient, ***hν*** corresponds to the energy of the photon beam, ***B*** is a constant parameter associated with creating new energy bands, and ***Eg*** represents the optical band gap energy. The parameter γ can take pairs of half-integer values, such as 1/2 and 3/2, representing electron transitions of direct allowed and direct forbidden nature, respectively. It can also take pairs of integer values, such as 2 and 3, denoting indirect allowed and indirect forbidden transitions, respectively. The extrapolated linear components of the plot of $\mathbf{(\alpha h\upsilon)^{1/\gamma}}$ intersecting the photon energy axis (x-axis) are utilized to determine the direct optical energy band gap of the polymer composite films. Table 3 presents the corresponding ***Eg*** values for all possible transitions. Based on the Taucs model, the $\boldsymbol{E_g}$ value was reduced to 1.52 and 1.78, corresponding to direct and forbidden selection. The dominant or exact type of transition could be specified in the later section of $\boldsymbol{\varepsilon_2}$ study versus photon energy, which is a subject related to condensed matter physics from the viewpoint of quantum physics. A recent study indicated that polymers with $\boldsymbol{E_g}$ less than 1.6 eV are decisive for various applications, including photonics, photovoltaics, transistors, and optoelectronics. The results of the current work are of great importance compared to those published in the literature. Recently, Abdel Fattah et al. [64], tried to shrink PVC's energy band gap (Eg) through the insertion of MWCNTs. In their study, they used plasma to develop the compatibility of MWCNTs with PVC matrix, thus reducing the E_g to 2 eV. Kassem et al. [65], studied the role of $BiVO_4$ nanomaterial on PVC's optical and shielding properties. They found that PVC's Eg (4.17–4.097 eV) was not influenced significantly. This work utilized green synthesis, and the E_g value was reduced to 1.52, a successful method in optical materials. Moreover; Al-Muntaser et al. [44], studied the role of $Li_4Ti_5O_{12}$ NPs on band gap reduction of PVC/PMMA. They reported the band gap reduction upon adding NPs from 4.2 to 3.69. El-Sayed et al. [66], also observed little reduction of PVAc/PVC from 4.22 to 3.97 eV

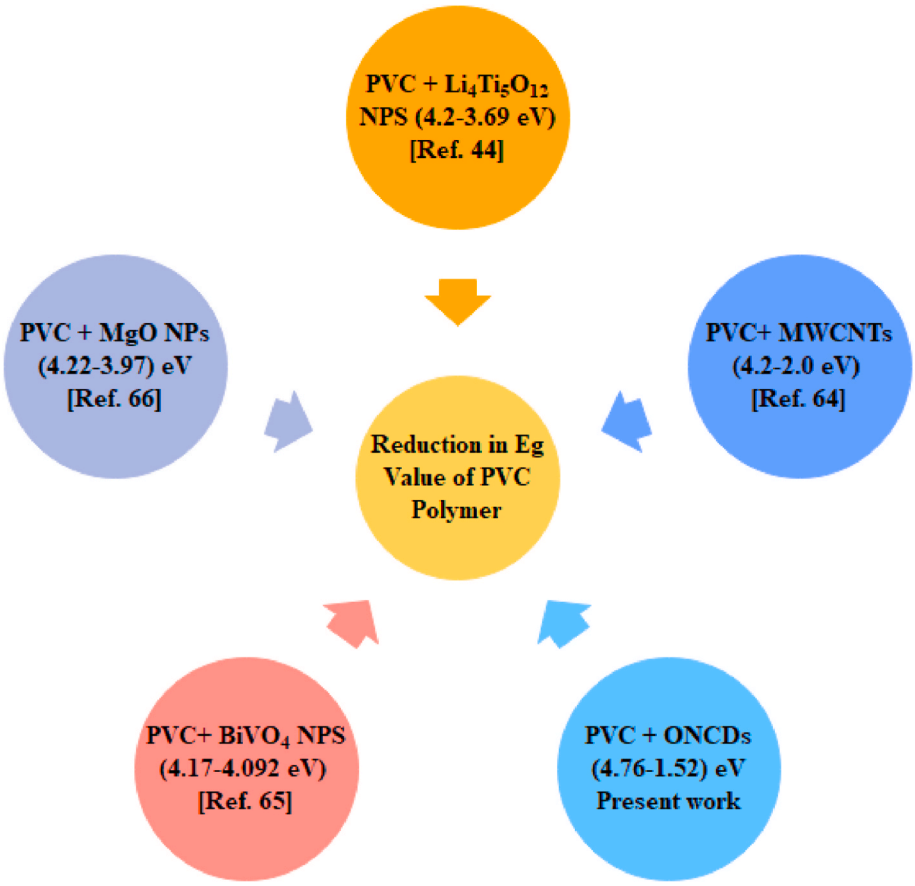

Scheme 2. Various materials to reduce the band gap of PVC.

upon inserting various MgO NPs. The findings of this study demonstrate that the incorporation of ONCDs can significantly impact the band gap of materials. The presence of ONCDs introduces a high density of localized states within the band gap, causing an overlap that reduces the region where electrons typically transition from the valence band to the conduction band. Additionally, it can be inferred that ONCDs have a more significant influence on modifying the optical band gap of weakly polar polymers like PVC compared to the attempts made with irradiation and ceramic nanoparticles. Further investigation in this field is necessary to confirm the exceptional ability of ONCDs to decrease the band gap in weakly polar organic polymers effectively. A significant contribution of this work is the utilization of ONCDs as a non-toxic and heavy metal-free material. Scheme 2 illustrates the role of various materials in changing the optical band gap of PVC polymer. Compared to various nano-materials, it can be seen that ONCDs are outstanding in changing the optical properties of PVC polymers. One more interesting point is that ONCDs are too flexible compared to neat PVC, which is almost brittle and transparent. The findings of this study, which employ an environmentally friendly methodology, have a clear and significant impact on the overall optical properties of PVC. From the outcomes of this innovative work, it can be understood that combining various fields of study, such as chemistry and physics, may produce scientific innovation essential for various technology applications. The development of low-cost polymer composites with enhanced optical properties has become a subject of considerable interest. Polymer composites, including wide band gap PVC, have attracted significant research attention worldwide. PVC, being a thermoplastic polymer, is particularly noteworthy due to its widespread use, affordability, and stability when compared to conductive polymers.

Predicting whether a band in amorphous materials will be of the direct or indirect type is challenging due to the diverse orbital contributions from both the dopants and the ligand [57]. Interband transitions are often not allowed inside the visible light spectrum because insulators typically have significant electronic band gaps. Here, the dielectric constant remains almost unaltered [67]. In theory, the dielectric function accounts for all phenomena intrinsic to how light and matter interact [68]. Previous studies have shown that the transfer of electrons from the valence band to the conduction band is responsible for the significant peak in ε_2 diagrams [57,69]. It is commonly recognized that amorphous materials exhibit broad peaks in the fundamental absorption region, while crystalline materials demonstrate sharper absorption characteristics. In our previous work [70], we noticed distinct peaks in the plot of the ε_2 parameter. The ε_2 is strongly correlated with the band structure of the materials, and this has been the subject of several theoretical quantum mechanical analyses [71–73]. The estimation of the optical band gap is possible through **equation (6)**, which relies on the electronic band structure, the density of states for filled and empty states, and the magnitude of the optical transition probability between them [67,74]:

$$\varepsilon_2(\omega) = \frac{4\pi^2}{\Omega\omega^2} \sum_{i\in VB, j\in CB} \sum_{K} W_K \left| p_{ij}^{a} \right|^2 \delta\left(\in_{kj} - \in_{ki} - \omega\right) \tag{6}$$

Where **Ω** represents the volume of a unit cell, **ω** denotes the frequency of light, VB and CB refer to the valence and conduction bands, respectively, $\mathbf{w_k}$ represents the weight associated with a specific k-point p_{ij}^{a} denotes the probability of a transition, and **a** represents the direction involved in the calculation. The delta function ensures energy conservation in electronic transitions, stipulating that the energy of a photon must precisely match the energy gap between a valence and conduction state for the transfer to occur. Using **equation (6)** to deduce the optical band gap, the relationship between the band structure of materials and the

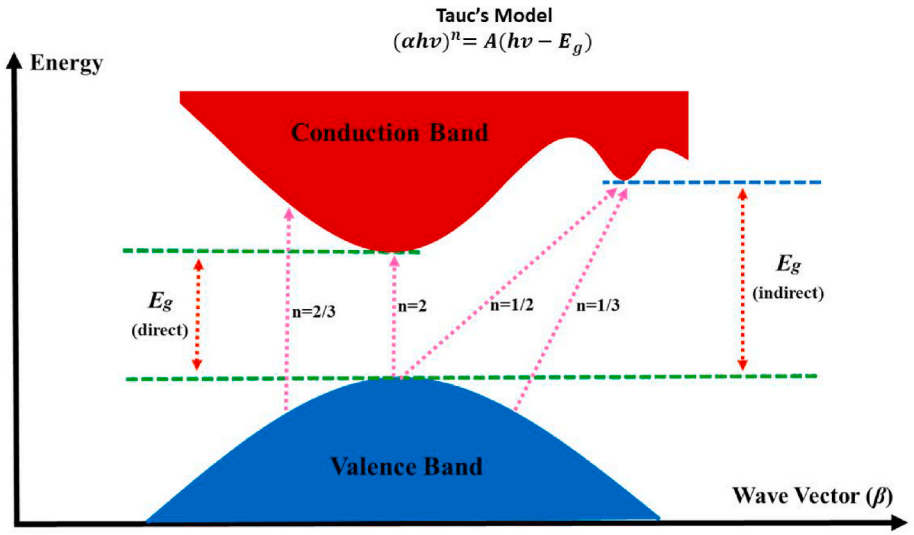

Fig. 17. Type of electronic transitions.

optical dielectric loss becomes evident. With the use of the measured refractive index **(n)** and extinction coefficient (K) ($\varepsilon_2 = 2$ nK), we were able to accurately predict the optical band gap in our previous studies [75]. Quantum mechanical applications of **Equation (6)** need elaborate numerical processes and models since they represent a microscopic method of investigating band gaps. The macroscopic approach of determining the optical band gap using optical dielectric loss ($\varepsilon_2 = 2$ nK) is quick and easy to implement and produces very accurate results [76]. As can be seen in Table 3, the gaps optical band gaps from the $\boldsymbol{\varepsilon_2}$ spectra are suitably secure to those estimated using the Taucs technique. Table 3 shows that in order to analyze the $\boldsymbol{E_g}$ between the VB and CB, the optical $\boldsymbol{\varepsilon_2}$ parameter is essential, while the Taucs approach is necessary in order to determine the various transitions that an electron can employ to overcome this barrier. The manipulation of newly formed levels between the valence band and conduction band of PVC is demonstrated by the reduction in $\boldsymbol{E_g}$ from 4.76 eV for the neat PVC to 1.52 eV for the doped PVC. The observed reduction further confirms the presence of permanent defects at the band edge within the prohibited band. Electronic transition types can be determined by comparing the $\boldsymbol{E_g}$ values obtained from Tauc's method (refer to Figs. 14 and 15) with those presented in Fig. 16. From a logical standpoint, one can deduce that the electronic transition type in neat PVC is directly allowed, whereas it becomes directly forbidden in PVC/ONCDs samples. This distinction may arise from the presence of crystalline domains that dominate the direct transition in neat PVC. In crystalline materials, the valence band (VB) aligns with the conduction band (CB), whereas this alignment does not occur in amorphous materials. This observation is supported by the XRD analysis, which revealed an increased amorphous phase in PVC/ONCDs composites compared to pure PVC. Schematically the types of electron transition belonging to direct and indirect are shown in Fig. 17.

4. Conclusion

The main conclusion of the current project demonstrates that organic soluble polar polymers, which are normally insulating, can be transformed into semiconducting materials by incorporating organic soluble nitrogen-doped carbon dots (ONCDs). This study successfully synthesized a novel green emissive ONCDs, exhibiting an average particle size distribution of around 9 nm. The synthesis was achieved using a solvent-free method, which resulted in a high yield of 50 % and a quantum yield of 10 % from 4-aminoantipyrine. Spectroscopic analysis showed that self-condensation reactions and noncovalent π-π stacking interactions were involved in the formation of ONCDs. The synthesized ONCDs were effectively employed to decrease the optical band gap of PVC polymer, presenting opportunities for improving the efficiency of optoelectronic devices. The PVC/ONCDs composite films exhibited improved optical properties, such as increased light absorption from UV to near-infrared range and a variable refractive index (1.72–216). The optical dielectric constant (2.9–4.6) also increased, indicating a higher localized density of states. The mechanism of band gap reduction and electron transition was elucidated by analyzing optical dielectric loss and applying the Taucs model. The outcome of this study presents an easy, high-yield, and cost-effective method for synthesizing ONCDs and demonstrates their potential for reducing the optical band gap of PVC polymer. This breakthrough enables the development of advanced polymer composites with tunable energy band gaps. The remarkable potential of low band gap PVC/ONCDs films extends to a wide range of optoelectronic devices, including solar cells, transistors, diodes, and lasers. Moreover low band gap polymer composites are crucial for laser power attenuation, optical limiters and laser sensors. Consequently, these findings offer exciting prospects for developing innovative technologies.

Funding

This research received no external funding

CRediT authorship contribution statement

Sewara J. Mohammed: Conceptualization, Data curation, Formal analysis, Investigation, Methodology, Project administration, Validation, Writing – original draft. **Farouq E. Hawaiz:** Conceptualization, Project administration, Supervision, Writing – review & editing. **Shujahadeen B. Aziz:** Conceptualization, Methodology, Resources, Writing – review & editing. **Sabah H Al-Jaf:** Conceptualization, Writing – review & editing.

Declaration of competing interest

The authors declare that they have no known competing financial interests or personal relationships that could have appeared to influence the work reported in this paper.

Data availability

Data will be made available on request.

Acknowledgments

The authors thank the University of Sulaimani for the scientific support to accomplish this research.

Appendix A. Supplementary data

Supplementary data to this article can be found online at https://doi.org/10.1016/j.optmat.2024.115014.

References

[1] A. Patra, C.G. Chandaluri, T.P. Radhakrishnan, Optical materials based on molecular nanoparticles, Nanoscale 4 (2012) 343–359, https://doi.org/10.1039/c1nr11313e.
[2] Z. Guo, A.A. Poot, D.W. Grijpma, Advanced polymer-based composites and structures for biomedical applications, Eur. Polym. J. 149 (2021), https://doi.org/10.1016/j.eurpolymj.2021.110388.
[3] A. Barabash, D. Barabash, V. Pertsev, D. Panfilov, Polymer-composite materials for radiation protection, Adv. Intell. Syst. Comput. 983 (2019) 352–360, https://doi.org/10.1007/978-3-030-19868-8_36.
[4] S. Kumar, Recent developments of biobased plasticizers and their effect on mechanical and thermal properties of poly(vinyl chloride): a review, Ind. Eng. Chem. Res. 58 (2019) 11659–11672, https://doi.org/10.1021/acs.iecr.9b02080.
[5] A. Turner, M. Filella, Polyvinyl chloride in consumer and environmental plastics, with a particular focus on metal-based additives, Environ. Sci. Process. Impacts 23 (2021) 1376–1384, https://doi.org/10.1039/d1em00213a.
[6] R.B. Carlos, M.R. Abreu, Talita C. Rezende, Armenio C. Serra, Ana C. Fonseca, J.F. J. Coelho, Convenient and industrially viable internal plasticization of poly(vinyl chloride): copolymerization of vinyl chloride and commercial monomers, Polymer 267 (2023) 125688, https://doi.org/10.1016/j.polymer.2023.125688.
[7] M. Hajibeygi, M. Maleki, M. Shabanian, F. Ducos, H. Vahabi, New polyvinyl chloride (PVC) nanocomposite consisting of aromatic polyamide and chitosan modified ZnO nanoparticles with enhanced thermal stability, low heat release rate and improved mechanical properties, Appl. Surf. Sci. 439 (2018) 1163–1179, https://doi.org/10.1016/j.apsusc.2018.01.255.
[8] S. Roy, M. David-Pur, Y. Hanein, Carbon nanotube-based ion selective sensors for wearable applications, ACS Appl. Mater. Interfaces 9 (2017) 35169–35177, https://doi.org/10.1021/acsami.7b07346.
[9] L. Jiang, J. Fu, L. Liu, P. Du, Wear and thermal behavior of basalt fiber reinforced rice husk/polyvinyl chloride composites, J. Appl. Polym. Sci. 138 (2021) 1–7, https://doi.org/10.1002/app.50094.
[10] S. Parola, B. Julián-López, L.D. Carlos, C. Sanchez, Optical properties of hybrid organic-inorganic materials and their applications, Adv. Funct. Mater. 26 (2016) 6506–6544, https://doi.org/10.1002/adfm.201602730.
[11] M.J. Cho, S.Y. Park, Preparation of poly(styrene)-b-poly(acrylic acid)-coupled carbon dots and their applications, ACS Appl. Mater. Interfaces 9 (2017) 24169–24178, https://doi.org/10.1021/acsami.7b04942.
[12] S. Anwar, H. Ding, M. Xu, X. Hu, Z. Li, J. Wang, L. Liu, L. Jiang, D. Wang, C. Dong, M. Yan, Q. Wang, H. Bi, Recent advances in synthesis, optical properties, and biomedical applications of carbon dots, ACS Appl. Bio Mater. 2 (2019) 2317–2338, https://doi.org/10.1021/acsabm.9b00112.
[13] J. Liu, R. Li, B. Yang, Carbon dots: a new type of carbon-based nanomaterial with wide applications, ACS Cent. Sci. (2020), https://doi.org/10.1021/acscentsci.0c01306.
[14] X. Li, S. Zhang, S.A. Kulinich, Y. Liu, H. Zeng, Engineering surface states of carbon dots to achieve controllable luminescence for solid-luminescent composites and sensitive Be2+ detection, Sci. Rep. 4 (2014) 1–8, https://doi.org/10.1038/srep04976.
[15] M.O. Alas, F.B. Alkas, A. Aktas Sukuroglu, R. Genc Alturk, D. Battal, Fluorescent carbon dots are the new quantum dots: an overview of their potential in emerging technologies and nanosafety, J. Mater. Sci. 55 (2020) 15074–15105, https://doi.org/10.1007/s10853-020-05054-y.
[16] J. Uchida, Y. Takahashi, T. Katsurao, H. Sakabe, One-step solvent-free synthesis of carbon dot-based layered composites exhibiting color-tunable photoluminescence, RSC Adv. 12 (2022) 8283–8289, https://doi.org/10.1039/d2ra00312k.
[17] Z. Zhang, X. Chen, G. Fang, J. Wu, A. Gao, Self-carbonization synthesis of highly-bright red/near-infrared carbon dots by solvent-free method, J. Mater. Chem. C (2022), https://doi.org/10.1039/d1tc05782k.
[18] Y. Sun, J. Liu, X. Pang, X. Zhang, J. Zhuang, H. Zhang, C. Hu, M. Zheng, B. Lei, Y. Liu, Temperature-responsive conversion of thermally activated delayed fluorescence and room-temperature phosphorescence of carbon dots in silica, J. Mater. Chem. C 8 (2020) 5744–5751, https://doi.org/10.1039/d0tc00507j.
[19] K.A.S. Fernando, S. Sahu, Y. Liu, W.K. Lewis, E.A. Guliants, A. Jafariyan, P. Wang, C.E. Bunker, Y.P. Sun, Carbon quantum dots and applications in photocatalytic energy conversion, ACS Appl. Mater. Interfaces 7 (2015) 8363–8376, https://doi.org/10.1021/acsami.5b00448.
[20] H. Li, S. Ye, J. Guo, H. Wang, W. Yan, J. Song, J. Qu, Biocompatible carbon dots with low-saturation-intensity and high-photobleaching-resistance for STED nanoscopy imaging of the nucleolus and tunneling nanotubes in living cells, Nano Res. 12 (2019) 3075–3084, https://doi.org/10.1007/s12274-019-2554-x.
[21] V. Sharma, P. Tiwari, S.M. Mobin, Sustainable carbon-dots: recent advances in green carbon dots for sensing and bioimaging, J. Mater. Chem. B 5 (2017) 8904–8924, https://doi.org/10.1039/c7tb02484c.
[22] Y. Liu, P. Wang, K.A. Shiral Fernando, G.E. Lecroy, H. Maimaiti, B.A. Harruff-Miller, W.K. Lewis, C.E. Bunker, Z.L. Hou, Y.P. Sun, Enhanced fluorescence properties of carbon dots in polymer films, J. Mater. Chem. C 4 (2016) 6967–6974, https://doi.org/10.1039/c6tc01932c.
[23] Y. Han, L. Liccardo, E. Moretti, H. Zhao, A. Vomiero, Synthesis, optical properties and applications of red/near-infrared carbon dots, J. Mater. Chem. C 10 (2022) 11827–11847, https://doi.org/10.1039/d2tc02044k.
[24] Y. Zhou, D. Benetti, X. Tong, L. Jin, Z.M. Wang, D. Ma, H. Zhao, F. Rosei, Colloidal carbon dots based highly stable luminescent solar concentrators, Nano Energy 44 (2018) 378–387, https://doi.org/10.1016/j.nanoen.2017.12.017.
[25] A. Kovalchuk, K. Huang, C. Xiang, A.A. Martí, J.M. Tour, Luminescent polymer composite films containing coal-derived graphene quantum dots, ACS Appl. Mater. Interfaces 7 (2015) 26063–26068, https://doi.org/10.1021/acsami.5b06057.
[26] S. Hu, Y. Ding, Q. Chang, A. Trinchi, K. Lin, J. Yang, J. Liu, Self-assembly of fluorescent carbon dots in a N,N-dimethylmethanamide solution via Schiff base reaction, Nanoscale 7 (2015) 4372–4376, https://doi.org/10.1039/c4nr07119k.
[27] Y. Zheng, D. Yang, X. Wu, H. Yan, Y. Zhao, B. Feng, K. Duan, J. Weng, A facile approach for the synthesis of highly luminescent carbon dots using vitamin-based small organic molecules with benzene ring structure as precursors, RSC Adv. 5 (2015) 90245–90254, https://doi.org/10.1039/x0xx00000x.
[28] G. Caputo, N. Pinna, Nanoparticle self-assembly using π-π Interactions, J. Mater. Chem. A 1 (2013) 2370–2378, https://doi.org/10.1039/c2ta00534d.
[29] S.J. Mohammed, K.M. Omer, F.E. Hawaiz, Deep insights to explain the mechanism of carbon dot formation at various reaction times using the hydrothermal technique: FT-IR, 13C-NMR, 1H-NMR, and UV-visible spectroscopic approaches, RSC Adv. 13 (2023) 14340–14349, https://doi.org/10.1039/d3ra01646c.
[30] D. Qu, Z. Sun, M. Zheng, J. Li, Y. Zhang, G. Zhang, H. Zhao, X. Liu, Z. Xie, Three colors emission from S,N Co-doped graphene quantum dots for visible light H2 production and bioimaging, Adv. Opt. Mater. (2015), https://doi.org/10.1002/adom.201400549.
[31] J. Wu, W. Wang, Z. Wang, Porphin-based carbon dots for "Turn off–on" phosphate sensing and cell imaging, Nanomaterials 10 (2020) 1–16, https://doi.org/10.3390/nano10020326.
[32] G.G. Lara, G.F. Andrade, M.F. Cipreste, W.M. da Silva, P.L. Gastelois, D.A. Gomes, M.C. de Miranda, W.A. de Almeida Macedo, M.J. Neves, E.M.B. de Sousa, Protection of normal cells from irradiation bystander effects by silica-flufenamic acid nanoparticles, J. Mater. Sci. Mater. Med. 29 (2018), https://doi.org/10.1007/s10856-018-6134-5.
[33] B. De, N. Karak, A green and facile approach for the synthesis of water soluble fluorescent carbon dots from banana juice, RSC Adv. 3 (2013) 8286–8290, https://doi.org/10.1039/c3ra00088e.
[34] J.M. Arroyave, R.E. Ambrusi, Y. Robein, M.E. Pronsato, G. Brizuela, M.S. Di Nezio, M.E. Centurión, Carbon dots structural characterization by solution-state NMR and UV–visible spectroscopy and DFT modeling, Appl. Surf. Sci. (2021), https://doi.org/10.1016/j.apsusc.2021.150195.
[35] L. Li, Y. Li, Y. Ye, R. Guo, A. Wang, G. Zou, H. Hou, X. Ji, Kilogram-scale synthesis and functionalization of carbon dots for superior electrochemical potassium storage, ACS Nano 15 (2021) 6872–6885, https://doi.org/10.1021/acsnano.0c10624.
[36] S.A. Hill, D. Benito-Alifonso, D.J. Morgan, S.A. Davis, M. Berry, M.C. Galan, Three-minute synthesis of sp3 nanocrystalline carbon dots as non-toxic fluorescent platforms for intracellular delivery, Nanoscale 8 (2016) 18630–18634, https://doi.org/10.1039/c6nr07336k.
[37] S.Y. Song, K.K. Liu, Q. Cao, X. Mao, W.B. Zhao, Y. Wang, Y.C. Liang, J.H. Zang, Q. Lou, L. Dong, C.X. Shan, Ultraviolet phosphorescent carbon nanodots, Light Sci. Appl. 11 (2022) 1–11, https://doi.org/10.1038/s41377-022-00837-1.
[38] S. Chahal, J.R. Macairan, N. Yousefi, N. Tufenkji, R. Naccache, Green synthesis of carbon dots and their applications, RSC Adv. 11 (2021) 25354–25363, https://doi.org/10.1039/d1ra04718c.
[39] W.U. Khan, D. Wang, W. Zhang, Z. Tang, X. Ma, X. Ding, S. Du, Y. Wang, High quantum yield green-emitting carbon dots for Fe(III) detection, biocompatible fluorescent ink and cellular imaging, Sci. Rep. 7 (2017) 1–9, https://doi.org/10.1038/s41598-017-15054-9.
[40] S. Bhattacharya, R.S. Phatake, S. Nabha Barnea, N. Zerby, J.J. Zhu, R. Shikler, N. G. Lemcoff, R. Jelinek, Fluorescent self-healing carbon dot/polymer gels, ACS Nano 13 (2019) 1433–1442, https://doi.org/10.1021/acsnano.8b07087.
[41] Y. Xiong, M. Chen, Z. Mao, Y. Deng, J. He, H. Mu, P. Li, W. Zou, Q. Zhao, Synthesis of up-conversion fluorescence N-doped carbon dots with high selectivity and sensitivity for detection of Cu2+ ions, Crystals 13 (2023), https://doi.org/10.3390/cryst13050812.
[42] P. Wu, W. Li, Q. Wu, Y. Liu, S. Liu, Hydrothermal synthesis of nitrogen-doped carbon quantum dots from microcrystalline cellulose for the detection of Fe3+ ions in an acidic environment, RSC Adv. (2017), https://doi.org/10.1039/c7ra08400e.
[43] S. Mallakpour, E. Shafiee, The synthesis of poly(Vinyl chloride) nanocomposite films containing ZrO2 nanoparticles modified with vitamin B1 with the aim of improving the mechanical, thermal and optical properties, Des, Monomers Polym. 20 (2017) 378–388, https://doi.org/10.1080/15685551.2016.1273436.
[44] A.A. Al-Muntaser, A.M. Abdelghany, E.M. Abdelrazek, A.G. Elshahawy, Enhancement of optical and electrical properties of PVC/PMMA blend films doped with Li4Ti5O12 nanoparticles, J. Mater. Res. Technol. 9 (2020) 789–797, https://doi.org/10.1016/j.jmrt.2019.11.019.

[45] G. Shimoga, E.J. Shin, S.Y. Kim, Thermal, dielectric and catalytic behavior of palladium doped PVC films, Polimeros 29 (2019) 1–9, https://doi.org/10.1590/0104-1428.08718.
[46] A.M. Abdelghany, M.S. Meikhail, N. Asker, Synthesis and structural-biological correlation of PVC\PVAc polymer blends, J. Mater. Res. Technol. 8 (2019) 3908–3916, https://doi.org/10.1016/j.jmrt.2019.06.053.
[47] H.B. Tahir, R.M. Abdullah, S.B. Aziz, The H+ ion transport study in polymer blends incorporated with ammonium nitrate: XRD, FTIR, and electrical characteristics, Results Phys. (2022), https://doi.org/10.1016/j.rinp.2022.105960.
[48] R. Kumar, S.A. Ali, A.K. Mahur, H.S. Virk, F. Singh, S.A. Khan, D.K. Avasthi, R. Prasad, Study of optical band gap and carbonaceous clusters in swift heavy ion irradiated polymers with UV-Vis spectroscopy, Nucl. Instrum. Methods Phys. Res. Sect. B Beam Interact. Mater. Atoms 266 (2008) 1788–1792, https://doi.org/10.1016/j.nimb.2008.01.010.
[49] Y. Wang, A. Hu, Carbon quantum dots: synthesis, properties and applications, J. Mater. Chem. C (2014), https://doi.org/10.1039/c4tc00988f.
[50] G. Yang, X. Wan, Y. Liu, R. Li, Y. Su, X. Zeng, J. Tang, Luminescent poly(vinyl alcohol)/carbon quantum dots composites with tunable water-induced shape memory behavior in different pH and temperature environments, ACS Appl. Mater. Interfaces 8 (2016) 34744–34754, https://doi.org/10.1021/acsami.6b11476.
[51] S.H. Deshmukh, D.K. Burghate, S.N. Shilaskar, G.N. Chaudhari, P.T. Deshmukh, Optical properties of polyaniline doped PVC-PMMA thin films, Indian J. Pure Appl. Phys. 46 (2008) 344–348.
[52] S.A. Saq'an, A.S. Ayesh, A.M. Zihlif, E. Martuscelli, G. Ragosta, Physical properties of polystyrene/alum composites, Polym. Test. 23 (2004) 739–745, https://doi.org/10.1016/j.polymertesting.2004.04.008.
[53] S.B. Aziz, H.M. Ahmed, A.M. Hussein, A.B. Fathulla, R.M. Wsw, R.T. Hussein, Tuning the absorption of ultraviolet spectra and optical parameters of aluminum doped PVA based solid polymer composites, J. Mater. Sci. Mater. Electron. 26 (2015) 8022–8028, https://doi.org/10.1007/s10854-015-3457-6.
[54] V.R.K. Hareesh, G. Sanjeev, A.K. Pandey, Characterization of UV-irradiated Lexan polycarbonate films, Iran. Polym. J. (Engl. Ed.) 22 (2013) 341–349.
[55] V. Bhavsar, D. Tripathi, Study of refractive index dispersion and optical conductivity of PPy doped PVC films, Indian J. Pure Appl. Phys. 54 (2016) 105–110.
[56] V.B. Kumar, A.K. Sahu, A.S.M. Mohsin, X. Li, A. Gedanken, Refractive-index tuning of highly fluorescent carbon dots, ACS Appl. Mater. Interfaces 9 (2017) 28930–28938, https://doi.org/10.1021/acsami.7b08985.
[57] S.B. Aziz, R.T. Abdulwahid, H.A. Rsaul, H.M. Ahmed, In situ synthesis of CuS nanoparticle with a distinguishable SPR peak in NIR region, J. Mater. Sci. Mater. Electron. 27 (2016) 4163–4171, https://doi.org/10.1007/s10854-016-4278-y.
[58] T.G. Urs, G.K. Gowtham, M.B. Nandaprakash, D. Mahadevaiah, Y. Sangappa, R. Somashekar, Determination of force constant and refractive index of a semiconducting polymer composite using UV/visible spectroscopy: a new approach, Indian J. Phys. 91 (2017) 53–56, https://doi.org/10.1007/s12648-016-0905-y.
[59] R. Pötzsch, B.C. Stahl, H. Komber, C.J. Hawker, B.I. Voit, High refractive index polyvinylsulfide materials prepared by selective radical mono-addition thiol-yne chemistry, Polym. Chem. 5 (2014) 2911–2921, https://doi.org/10.1039/c3py01740k.
[60] I. Saini, J. Rozra, N. Chandak, S. Aggarwal, P.K. Sharma, A. Sharma, Tailoring of electrical, optical and structural properties of PVA by addition of Ag nanoparticles, Mater. Chem. Phys. 139 (2013) 802–810, https://doi.org/10.1016/j.matchemphys.2013.02.035.
[61] O.W. Guirguis, M.T.H. Moselhey, Optical study of poly(vinyl alcohol)/hydroxypropyl methylcellulose blends, J. Mater. Sci. 46 (2011) 5775–5789, https://doi.org/10.1007/s10853-011-5533-5.
[62] V. Krishnakumar, S. Govindaraj, Electrical and optical properties of pure and Pb 2 + ion doped PVA − PEG polymer composite electrolyte films, Ionics 18 (2011) 403–411, https://doi.org/10.1007/s11581-011-0643-2.
[63] K.S. Hemalatha, K. Rukmani, N. Suriyamurthy, B.M. Nagabhushana, Synthesis, characterization and optical properties of hybrid PVA-ZnO nanocomposite: a composition dependent study, Mater. Res. Bull. 51 (2014) 438–446, https://doi.org/10.1016/j.materresbull.2013.12.055.
[64] T.F.E. Abdel-Fattah, A.I. Alharthi, Spectroscopic, optical and thermal characterization of polyvinyl chloride-based plasma-functionalized MWCNTs composite thin flms, Appl. Phys. A 125 (2019) 475, https://doi.org/10.1007/s00339-019-2770-y.
[65] S.M. Kassem, M.I.A. Abdel Maksoud, A.M. El Sayed, S. Ebraheem, A.I. Helal, Y. Y. Ebaid, Optical and radiation shielding properties of PVC/BiVO4 nanocomposite, Sci. Rep. 13 (2023) 10964, https://doi.org/10.1038/s41598-023-37692-y.
[66] A.M.E. Sayed, A.M. Abdelghany, A. Abou Elfadl, Structural, optical, mechanical and antibacterial properties of MgO/Poly(Vinyl acetate)/poly(vinyl chloride) nanocomposites, Braz. J. Phys. 52 (2022), https://doi.org/10.1007/s13538-022-01156-x.
[67] H. Bao, X. Ruan, Ab initio calculations of thermal radiative properties: the semiconductor GaAs, Int. J. Heat Mass Tran. 53 (2010) 1308–1312, https://doi.org/10.1016/j.ijheatmasstransfer.2009.12.033.
[68] R. Alaya, S. Slama, M. Hashassi, M. Mbarki, A. Rebey, S. Alaya, Theoretical predictions of structural, electronic, and optical properties of dilute bismide AlN1−xBixin zinc-blend structures, J. Electron. Mater. 46 (2017) 1977–1983, https://doi.org/10.1007/s11664-017-5318-y.
[69] M. Wu, D. Sun, C. Tan, X. Tian, Y. Huang, Al-doped ZNO monolayer as a promising transparent electrode material: first-principles study, Materials 10 (2017), https://doi.org/10.3390/ma10040359.
[70] S.B. Aziz, O.G. Abdullah, M.A. Rasheed, A novel polymer composite with a small optical band gap: new approaches for photonics and optoelectronics, J. Appl. Polym. Sci. 134 (2017) 1–8, https://doi.org/10.1002/app.44847.
[71] C. Bouzidi, K. Horchani-Naifer, Z. Khadraoui, H. Elhouichet, M. Ferid, Synthesis, characterization and DFT calculations of electronic and optical properties of CaMoO4, Phys. B Condens. Matter 497 (2016) 34–38, https://doi.org/10.1016/j.physb.2016.06.009.
[72] J. Feng, B. Xiao, J.C. Chen, C.T. Zhou, Y.P. Du, R. Zhou, Optical properties of new photovoltaic materials: AgCuO2 and Ag2Cu2O3, Solid State Commun. 149 (2009) 1569–1573, https://doi.org/10.1016/j.ssc.2009.05.042.
[73] S. Logothetidis, Optical and electronic properties of amorphous carbon materials, Diam. Relat. Mater. 12 (2003) 141–150, https://doi.org/10.1016/S0925-9635(03)00015-3.
[74] M. Nematollahi, X. Yang, L.M.S. Aas, Z. Ghadyani, M. Kildemo, U.J. Gibson, T. W. Reenaas, Molecular beam and pulsed laser deposition of ZnS:Cr for intermediate band solar cells, Sol. Energy Mater. Sol. Cells 141 (2015) 322–330, https://doi.org/10.1016/j.solmat.2015.06.004.
[75] S.B. Aziz, M.M. Nofal, M.A. Brza, N.M. Sadiq, E.M.A. Dannoun, K.K. Ahmed, S.I. Al-Saeedi, S.A. Hussen, A.M. Hussein, Innovative green chemistry approach to synthesis of Sn2+-metal complex and design of polymer composites with small optical band gaps, Molecules 27 (2022), https://doi.org/10.3390/molecules27061965.
[76] A. Rodríguez, M.E. Sánchez Vergara, V. García Montalvo, A. Ortiz, J.R. Alvarez, Thin films of molecular materials synthesized from C 32 H 20 N 10 M (M = Co, Pb, Fe): film formation, electrical and optical properties, Appl. Surf. Sci. 256 (2010) 3374–3379, https://doi.org/10.1016/j.apsusc.2009.12.037.